

Using surface-enhanced Raman spectroscopy to probe for genetic markers on single-stranded DNA

Benjamin Moody

John Leotaud

Gregory S. McCarty

University of North Carolina, Chapel Hill

and

North Carolina State University

Joint Department of Biomedical Engineering

2140 Burlington Labs

2500 Stinson Drive

Raleigh, North Carolina 27695

Abstract. Methods capable of quickly and inexpensively collecting genetic information are of increasing importance. We report a method of using surface-enhanced Raman spectroscopy to probe single-stranded DNA for genetic markers. This unique approach is used to analyze unmodified genes of moderate length for genetic markers by hybridizing native test oligonucleotides into a surface-enhanced Raman complex, vastly increasing detection sensitivity as compared to traditional Raman spectroscopy. The Raman complex is formed by sandwiching the test DNA between 40-nm gold nanoparticles and a photolithographically defined gold surface. With this design, we are able to collect characteristic Raman spectra about the test DNA and to detect genetic markers such as single-nucleotide polymorphisms (SNPs) and polymorphic regions. Results show that strands containing one of three different types of polymorphism can be differentiated using statistically significant trends regarding Raman intensity. © 2010 Society of Photo-Optical Instrumentation Engineers. [DOI: 10.1117/1.3400702]

Keywords: genetic markers; Raman spectroscopy; polymorphisms; DNA.

Paper 10007R received Jan. 6, 2010; revised manuscript received Feb. 19, 2010; accepted for publication Mar. 4, 2010; published online Apr. 16, 2010.

1 Introduction

The detection of genetic markers has become ubiquitous in modern scientific research as a tool for examining the genetic relationships that underpin traits involving heredity, biological variability, disease susceptibility, and pharmacological efficacy, to name a few. Because DNA sequence variations such as single-nucleotide polymorphisms (SNPs) have been associated with approximately 90% of polymorphisms in the human genome,¹ researchers often use SNPs as markers for a variety of genetic diseases² and cancers.³

The importance of improving the speed, specificity, and cost efficiency of methodologies used to collect genetic information directly correlates with the importance of the information itself. Although polymorphisms as genetic markers are traditionally probed using time-intensive Southern blot hybridizations and polymerase chain reaction (PCR)-related methodologies,⁴ more recent innovations using DNA functionalized with gold nanoparticles (AuNPs) have made preliminary steps in detecting terminal DNA mismatches.⁵⁻¹⁰ In 2004, it was noted that single-stranded DNA oligonucleotides (oligos) can be functionalized to gold nanoparticles in separate solutions that each have an inherent pink color.⁵ When the nanoparticle solutions of DNA with mismatched terminal bases are mixed, the gold nanoparticles precipitate, and the solution loses its pink color. Unfortunately, researchers were not able to use this technique with mismatched bases closer to the middle of the sequence, and the test DNA had to be modified to attach the nanoparticles.⁵

Raman spectroscopy is another sensitive detection technique that has the potential of reducing the need for PCR and laborious biochemical techniques. Since the early 1970s, researchers have been using Raman to explore nearly every aspect of biology and biomedicine,^{7,8,10,11} including DNA.¹² While innately weak Raman signals, fluorescence, and large background noise can make biological Raman applications difficult, advances in laser and filter technology and the advent of surface-enhanced Raman spectroscopy (SERS) have improved Raman capabilities. Further, combinations of Raman spectroscopy with aspects of nanotechnology provide even greater utility.¹³ Combining gold nanoparticle-based SERS with DNA opens several avenues of pure DNA analysis and subsequent gene detection methodologies.¹⁴⁻¹⁷ Sun et al. have developed a way to detect breast cancer genes using the hybridization of sample DNA with probing DNA that has been modified with gold nanoparticles and specific Raman labels. Using this technique, Sun et al. were able to achieve detection sensitivities of down to 1 fM (Ref. 13).

Previous results from our lab used SERS to detect, with high levels of statistical confidence, differences between samples of complementary oligos and those formed from oligos with a midsequence base mismatch.¹⁸ However, a major drawback to the practical and clinical applicability of this technology is the need to add thiol modifications to each different oligo intended for analysis. Not only is it expensive to add thiol modifications to numerous test strands, the variability associated with the surface chemistry involved in functionalizing a large variety of oligonucleotides with gold nanoparticles gives rise to aggregation, precipitation, poor adsorption,

Address all correspondence to: Benjamin Moody, North Carolina State University, Biomedical Engineering, 2140 Burlington Labs, 2500 Stinson Drive, Raleigh, North Carolina 27695. Tel: 919-513-7933; Fax: 919-513-3814; E-mail: agsmccart@ncsu.edu

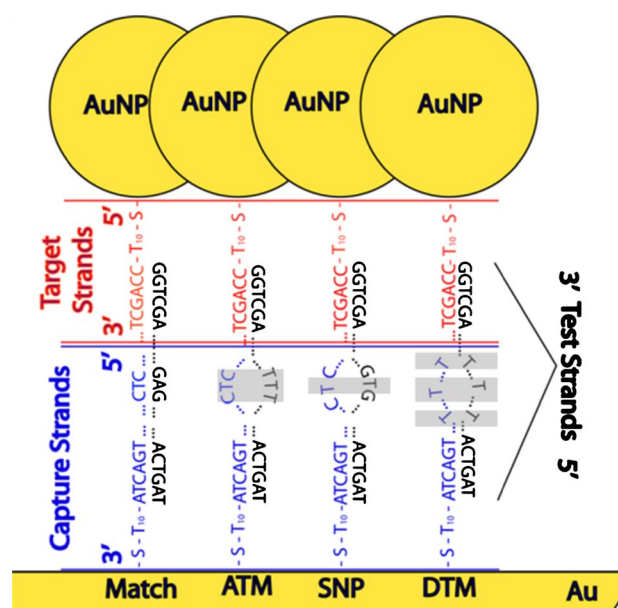


Fig. 1 Visualization of the hybridization scheme used to create an SERS environment around DNA duplexes. Single-stranded oligos are hybridized as either completely matched, with a single mismatch (SNP), with an adjacent triple mismatch (ATM), or with a delocalized triple mismatch (DTM). Gray boxes highlight the mismatches for clarity.

and other deleterious interactions with the gold nanoparticles. We have found that using a single modified detection oligo to test for multiple mutations reduces sample-to-sample variability, decreases the amount of preparation time, and decreases the need for costly reagents and modified DNA material.

In this paper, we refine and expand previous techniques to further investigate the technology's potential for genetic marker detection and to make the technology more applicable to biological studies. Namely, we have eliminated the need to directly functionalize the test oligo with gold nanoparticles, and we have expanded the capabilities of this technology to detect and explore two different types of polymorphic regions (PRs) in addition to lone SNP detection. The enhanced ability to test for multiple mutations along a native, unmodified gene broadens the applicability of this technique to practical genetic marker detection methodologies.

2 Materials and Methods

The overall idea is to capture single-stranded “test” oligonucleotides between closely spaced gold features. As depicted in Fig. 1, a DNA test strand can be probed for abnormal base mutations by hybridizing one highly conserved region of the strand to a gold surface-bound “capture” oligo and another region to a gold nanoparticle-bound “detection” oligo, thus creating a SERS environment around the test oligo. This was accomplished in a three-step aqueous hybridization procedure using preparations similar to those previously developed^{13,18} with several variations. Test samples were composed of the four types of DNA duplexes visualized in Fig. 1 and defined in Table 1—those formed from complementary oligos, those formed from oligos with a single midsequence base mismatch (SNP), those formed from oligos that have three delocalized

Table 1 Oligonucleotide design for matched and mismatched sequences.

	Sequence
Detection strand	5'—Thiol—T ₁₀ —CCA GCT TAGA—3'
Capture strand	5'—ATC GCA TGA GCT CAT ATG CAT CGA TGA CTA— T ₁₀ —Thiol—3'
Complementary	5'—GGT CGA ATC TTA GCG TAC TCG AGT ATA CGT AGC TAC TGAT—3'
Single mismatched	5'—GGT CGA ATC TTA GCG TAC TCG— T —GTA TAC GTA GCT ACT GAT—3'
Adjacent triple mismatched	5'—GGT CGA ATC TTA GCG TAC TC— TTT —TAT ACG TAG CTA CTG AT—3'
Delocalized triple mismatched	5'—GGT CGA ATC TT— T —GCG T— T —C TCG AGT— T — TAC GTA GCT ACT GAT—3'

mismatches (DTM), and those that have a polymorphic region of three adjacent mismatches (ATM). Resulting Raman spectra were compared for statistically significant intensity and peak position differences at four characteristic peaks as described later. The overall method involves nine main steps, as follows:

1. Wafer preparation. As described elsewhere,¹⁸ ~2–3- μm gold spots (400-nm Au on 30-nm chrome) situated in arrays of 20 spots per array are prepared on quartz wafers (SiliconQuest) using photolithography and electron-beam deposition. The wafer was treated with 30% wt% peroxide for 1 h immediately prior to spotting.

2. Capture strand preparation. 40-mer oligonucleotides with a 3' thiol modification were used as the capture strands. The sequence (5'—ATC GCA TGA GCT CAT ATG CAT CGA TGA CTA T₁₀—Thiol—3') was chosen with 10 thymine bases acting as a spacer^{13,19} immediately adjacent to the thiol modification, followed by 30 bases chosen to interact with the 30 bases on the 5' end of the test strands. Oligos were purified with a standard desalt during manufacturing. The use of spacers in this experiment increases the distance between mismatched bases and either gold surface to between 22 and 35 bases, or approximately 7 to 11 nm. This distance excludes the potential for direct DNA–gold interactions and reinforces the experimental design that fundamentally operates on the decreased binding affinity experienced by mismatched ssDNA strands as detected by SERS. Therefore, the use of spacers insures Raman detection of a mismatch should be relatively independent of proximity of that mismatch to either gold surface. The DNA capture solution was prepared by suspending dry DNA (Integrated DNA Technologies) in an aqueous solution of 10 mM Tris, 0.1 mM EDTA, buffered at pH 8.0. This solution will be referred to as IDTE. The concentration of DNA in solution was 1 μM . This solution was first reduced with Reductacryl (Calbiochem) and then spotted

onto micropatterned metal arrays on the quartz wafer, which was then placed in a humid environment and incubated for 6 h at room temperature.

3. Wafer functionalization. After incubation, the wafer was rinsed by multiple submersions in deionized (DI) water and dried under nitrogen. The wafer was then spotted with a 1 mM solution of mercapto-1-hexanol (MHOH; Sigma) in ethanol and allowed to sit overnight (~17 h) in order to limit nonspecific binding in later steps.^{13,20} MHOH was rinsed with DI water by immersion and dried under nitrogen.

4. Detection strand preparation. Detection strands were designed to be complementary to the last 10 bases on the 3' terminus of the test strands. Therefore, detection strands contained 20 bases—10 meant to hybridize with the linking strands and 10 thymine spacers—and a thiol modification on the 5' end. The procedure for functionalization with gold nanoparticles and hybridization with capture strands is similar to that developed by Sun et al., with some variations.¹³ The detection solution was prepared by adding concentrated DNA in IDTE to a solution of 40-nm gold nanoparticles (Ted Pella) such that the final DNA concentration of the detection solution was 10 μ M. After 24 h, the gold/oligo solution was buffered with a 10 mM pH 7.5 phosphate buffer, 0.15% tween solution (PB/T). After 30 min, the detection solution was salted by four additions of 20 μ L 4 M NaCl with vigorous mixing between additions to bring the final salt concentration to 0.3 M. After ~48 h, the detection solutions were washed in PB/T with 0.3 M NaCl twice, with centrifugations (and redispersing vortexes) between, and again brought up to 10 μ M in the same solution.

5. Test strand hybridization. Test strands were deemed complementary (matched), single mismatched (SNP), adjacent triple mismatched (ATM), delocalized triple mismatched (DTM), or noncomplementary (completely mismatched) based on how they matched to the capture strand, as described in Table 1. All mismatches were designed to be thymine–thymine or thymine–cytosine mismatches to minimize the possibility of alternate Watson–Crick base pairings such as the wobble structure. Test strands were also prepared by diluting the dry DNA to 1 μ M solutions in IDTE. Immediately following wafer functionalization (step 3), the test strands were spotted onto appropriate arrays, again put in a humid environment, and incubated at 40 °C for 4 h to ensure time for correct hybridization.¹³ The wafer was then rinsed by immersion in DI water and dried with nitrogen.

6. Detection hybridization. Last, detection strands were spotted onto the arrays, again put in a humid environment, and incubated at 40 °C for 4 h. The wafer was then rinsed with 10 mM PB/T and immersion rinsed in DI water and dried with nitrogen. Last, the wafer was soaked in Silver Enhance (Ted Pella) solution for 10 min, rinsed and dried again, and immediately analyzed with Raman. Further water rinses after 24 h did not have an effect on the Raman signal.

7. Raman detection. Raman scattering was excited using a 12-mW red HeNe laser (Thorlabs) coupled to an inverted microscope (Nikon, Diaphot) with a 60 \times dry objective (Olympus). The reflected Raman signal was analyzed through an imaging spectrograph (PI Acton, SpectraPro SP-2156) and detected with a liquid nitrogen–cooled CCD camera (PI Acton, Spec-10:100BR/LN). The laser power at the sample mea-

sured 3 mW, and the laser spot was about 2 μ m in diameter. Collection times were 20 s. GRAMS/AI 8.0 software (Thermo) was used to average the spectra and for baseline correction.

8. Statistical analysis. A two-sided, two-sample *t*-test ($\alpha=0.05$) assuming unequal variances was applied to the seven median intensity values of the selected peaks. For plotting, the seven median spectra were baseline subtracted using a constant offset (as opposed to the “rubber band method”) that consisted of a straight line from the local minimum (created by the laser line notch filter) in the spectrum at ~200 relative wave numbers to the local minimum at ~2000 relative wave numbers (past the region of observed Raman peaks). The spectra were then averaged and finally smoothed with a 5-point binomial smooth. The same *t*-test was also employed to determine significance in peak shifts except that peak positions were used in lieu of intensities. In this case, the peak intensities were also normalized prior to plotting (see Fig. 4, shown later) to more clearly represent the individual shifts.

9. Electron micrograph analysis. A visual characterization of the surface was accomplished in order to gain additional information regarding the mechanism behind the observed Raman enhancements and to validate the overall experimental model. Scanning electron micrographs (SEMs) were collected using a Joel 6400F SEM operating at a 5-keV accelerating voltage. Images were taken at each gold array that contained Raman information, and representative images were analyzed for particle count and particle density using ImageJ software.

3 Results

Twenty-four Raman spectra from each test sample were collected and processed as previously reported.¹⁸ To eliminate high and low outliers, subsets of 7 median spectra were selected from each original group of 24. These median subsets were averaged to determine overall intensity for plotting, and the intensities and peak positions of the four characteristic nucleic acid peaks were extracted for statistical analysis. Statistical significance was determined (from $p < 0.01$ to $p < 0.001$, $\alpha=0.05$) for differences between each of the samples at the four selected peaks. The characteristic peaks primarily included contributions from the two purine-containing nucleic acids, guanine and adenine, due to the increased cross-sectional areas and therefore increased SERS activity of these molecules.²¹ The four selected peaks were a guanine ring breathing at 660 cm^{-1} (Refs. 22 and 23), the phosphodiester backbone peak around 840 cm^{-1} (Ref. 24), a guanine stretch at 970 cm^{-1} (Refs. 22–24), and guanine/denine vibrations at 1174 cm^{-1} (Refs. 22 and 23). Figure 2 more succinctly shows the peak positions and standard error of these key peaks. Note that among all these peaks, the overall Raman intensity of the complementary sample is significantly greater than that of the single-mismatched sample, which is itself greater than the triple-mismatched samples. Significance levels are individually summarized in Table 2.

Scanning electron microscopy (SEM) images seen in Fig. 3 qualitatively support the theory that more nucleotides are being hybridized in complementary samples than in single-mismatched and multiple-mismatched samples. The figure shows greater surface area coverage of nanoparticles on the

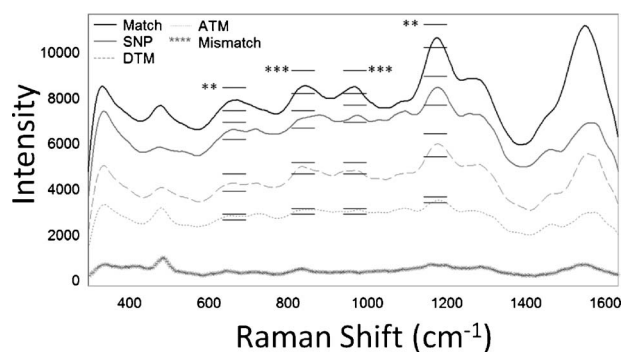


Fig. 2 Raman spectra comparing the averaged median intensities of single-stranded oligos (matched, single mismatched, delocalized triple mismatched, adjacent triple mismatched, and completely mismatched) hybridized to form double-stranded duplexes. Standard error bars are included for the key peaks. (See Table 2 for p -values.)

gold spot with complementary oligos and a reduced amount on the spots with mismatched oligos. Additionally, image analysis software (ImageJ) concludes that the percent coverage of nanoparticles in the representative areas is 25.0% for the matched sample, 17.8% for the SNP sample, and 14.1% for the triple-mismatched sample. The relatively small differences in nanoparticle coverage between samples are to be expected given that the binding affinities of mismatched samples are altered only by one to three base mutations as compared to the matched samples. Note that while these images show qualitative support for the Raman data, sample-to-sample variability in nanoparticle surface coverage limits subsequent significance analyses.

Figure 4 represents a magnification of the 500 to 1300 cm^{-1} area in Fig. 2. The three aforementioned peaks, highlighted and magnified further in Figs. 4(a)–4(c), show statistically significant peak shifts when comparing the average matched sample to the SNP and ATM samples. The DTM sample followed in trend with the other mismatched samples and was therefore excluded for clarity. Constituent peak heights were normalized to the peak of interest before averaging. It should be noted that while the average position among mismatched samples appears different in Fig. 4, this difference is not statistically significant and therefore will not be treated as meaningful. Only position shifts between the

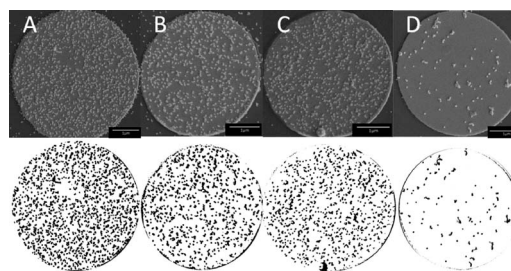


Fig. 3 Scanning electron micrographs of representative sample capture surfaces after hybridizing single-stranded oligos and gold nanoparticles to form double-stranded SERS complexes (top row). The bottom row contains corresponding particle count analyses that clarify the different particle densities of each micrograph. These images enable a qualitative analysis of the nanoparticle densities that results from hybridizing with (a) completely matched, (b) SNP, (c) triple-mismatched, and (d) completely mismatched test strands.

matched samples and the mismatched samples are statistically significant. Peak positions are shown with their respective standard errors and levels of significant difference as compared to the matched sample. Table 3 summarizes the significance level of each shift. Studies verify that these peak shifts are not affected by the surface coverage of nanoparticles.

4 Discussion

The effort of this paper is to extend the use of Raman spectroscopy to detect genetic markers on unmodified oligonucleotides and to determine the applicability of using this type of approach for exploring DNA hybridization characteristics associated with SNPs and PRs. There are two mechanisms behind the feasibility of these experiments. First, because genetic markers such as SNPs and PRs contain energetically unfavorable nucleotide mismatches in the DNA helix, mismatched oligos are less likely to hybridize as effectively as matched oligos and are more successfully removed with stringent washes. Because the creation of an SERS environment is dependent on the hybridization of oligos, mismatched samples have a decreased overall Raman signal that can be used to differentiate them from matched samples in a direct comparison analysis. Increasing the number of mismatches only amplifies this effect and further decreases the Raman signal. Second, it is proposed that hybridized samples with mismatches

Table 2 Two-tail p -values from t -test results used to test the significance of intensity differences among selected peaks. Asterisks represent corresponding significance levels of the sample comparisons as indicated.

		Comparison		
		Match/SNP	SNP/DTM	DTM/ATM
Relative peak position (cm^{-1})	660	5.19×10^{-3} **	6.06×10^{-5} ***	5.98×10^{-4} ***
	840	1.11×10^{-3} ***	5.45×10^{-5} ***	3.51×10^{-8} ***
	970	8.76×10^{-4} ***	2.18×10^{-5} ***	1.85×10^{-7} ***
	1170	4.80×10^{-4} ***	4.82×10^{-3} **	6.73×10^{-4} ***

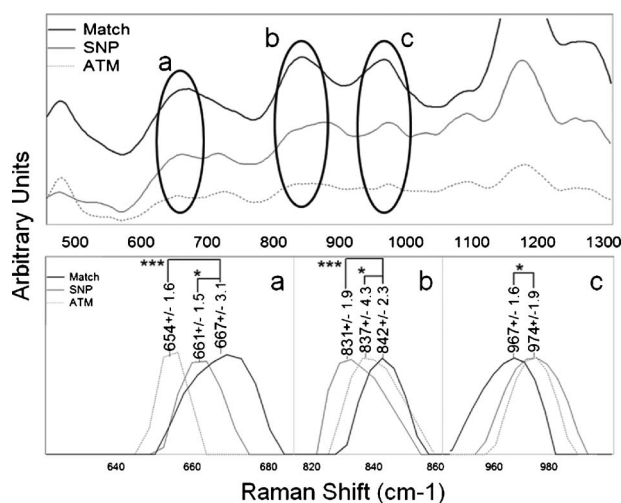


Fig. 4 Raman spectra highlighting the peak position shifts that occur when comparing the average matched sample to the SNP and ATM samples. The DTM sample followed in trend with the other mismatched samples and was therefore excluded for clarity. The highlighted peaks represent (a) down-shifting guanine ring breathing and (b) phosphodiester stretch modes and (c) an up-shifting guanine/sugar stretch. Peak positions are shown with their respective standard errors, representing the variability between the seven median spectra averaged together to obtain these positions. Levels of significant difference are compared to the matched sample. Constituent peak intensities were baseline subtracted and normalized to the peak of interest before averaging and then smoothed. (See Table 3 for p -values.)

are subject to altered intermolecular bonding patterns that affect characteristic vibration modes. Therefore, not only does the overall Raman intensity differ between matched and mismatched samples, the Raman signatures also give insight into the mismatch.

In accordance with the theoretical basis for this experiment and as shown in Figs. 2 and 3, it is to be expected that the SNP samples have a weaker Raman intensity than matched oligos and that multiple mismatches exhibit a weaker signal still. Based on free-energy calculations of single-stranded oligo hybridizations as described and tabulated by Turner et al.,²⁵ it is predicted that among the multiple-mismatched samples, the DTM will show a higher binding affinity than the ATM. These calculations assume that base-pair mismatches form energetically unfavorable internal loops within the helix

Table 3 Two-tail p -values from t -test results used to test the significance of peak position differences among selected peaks. Asterisks represent corresponding significance levels of the ATM and SNP samples as compared to the matched sample as indicated.

Relative peak position (cm^{-1})	Comparison	
	Match/SNP	Match/ATM
660	2.98×10^{-2} *	6.68×10^{-4} ***
840	2.05×10^{-4} ***	2.36×10^{-2} *
970	6.26×10^{-3} **	1.12×10^{-2} *

and infer that when predicting hybridization stability, both the size of the mismatch and the sequence position of the mismatch are important. In this case, not only would the DTM incur a lower cumulative energy penalty than the ATM but also the mismatches in the DTM are positioned such that they sacrifice fewer energetically favorable matches. Such calculations conclude that the energy difference between the two triple-mismatched samples is only 1.4 kcal in favor of DTM hybridization. Although Raman experiments were able to distinguish this difference significantly, as seen in Fig. 2, experimental conditions such as hybridization temperature, reagent concentration, DNA age, and quality of the photolithography must be tightly controlled for successful differentiation. It is proposed that such a small energy difference is very near the lower level of detection for this technique and that while these calculations give general theoretical reinforcement to the observed experimental trends, it should be noted that due to the nature of SERS enhancements, there is little quantifiable correlation between binding energies and Raman intensity. However, between the match, SNP, and triple mismatches in general, experimental Raman results show robust, consistent, and reproducible intensity trends. For comparison, free-energy calculations comparing DTM and SNP show a 5.5-kcal difference, and those comparing SNP and the complete match hybridization show a 4.8-kcal difference.

To further improve understanding of the system, observations were also made regarding peak positions in the Raman spectra seen in Figs. 2 and 4. The principal observation is a slight shift in the position of three of the characteristic peaks mentioned earlier—the guanine ring breathing peak at 660 cm^{-1} (Refs. 22 and 23), the phosphodiester backbone peak around 840 cm^{-1} (Ref. 24), and the guanine stretch at 970 cm^{-1} (Refs. 22–24). Because Raman spectroscopy is a fingerprint technique, each peak represents a specific molecular vibration that contains information about its local chemical environment. Therefore, additional information can be gained by observing shifts in peak position as they relate to molecular conformations, structural rearrangements, and other changes in the chemical environment.

Significant differences here can be used to gain insight into chemical changes that occur upon hybridization of mismatched oligos. Figure 4(a) shows that the phosphodiester peak at 842 cm^{-1} in the matched sample is conspicuously shifted to a lower wavelength (down-shifted) of around 831 cm^{-1} for the mismatched samples. It has been observed in previous studies that the phosphodiester band shifts from 835 cm^{-1} to 815 cm^{-1} as the order and rigidity of the system decreases from B-DNA to A-DNA to single-stranded oligonucleotides, respectively.²⁴ In other words, as the order and rigidity of the bond decreases, it takes less energy from an incident photon to induce the same vibrational mode. Empirically, this can be represented with the following equation:²⁶

$$\Delta E_{\text{photon}} = \Delta E_{\text{transition}} = \frac{h}{2\pi} \sqrt{\frac{k}{\mu}}, \quad (1)$$

or

$$\nu = \frac{1}{2\pi c} \sqrt{\frac{k}{\mu}}, \quad (2)$$

where h is Planck's constant, c is the speed of light, k is Hooke's law force constant for stretching the bond, ν is the Raman frequency shift for the associated vibration, and μ is the reduced mass of the two atoms whose bond is being affected.²⁶

Interestingly, Fig. 4(c) shows that the 967 cm⁻¹ peak associated with the bond stretch between guanine and its sugar is seen to shift to higher wavelengths in the SNP and ATM samples as compared to the matched sample. We speculate that breaking the hydrogen bonding pattern in the bases induces a more widespread redistribution in electron arrangement over the entire nucleotide that relaxes structural bonds near the backbone and strengthens those nearer to the base. In this case, the 967-cm⁻¹ peak shifts to approximately 974 cm⁻¹ in the two mismatched samples. In contrast, a vibrational mode not necessarily associated with nucleotide structure, guanine's imidazole ring-breathing mode related to the peak at 667 cm⁻¹, down-shifts to ~654 cm⁻¹ in the mismatched samples, again indicating a decreased sense of order within the ring. This final shift can be seen in Fig. 4(a). Again, there were no meaningful position shifts among the mismatched samples, only between the mismatched samples and the matched sample. Such observations attest to the varied amount of information that can be obtained from these types of Raman studies, extending the technique both as a robust polymorphism detection scheme for genotyping analyses and as a useful tool for analyzing additional minute and fundamental chemical relationships regarding DNA hybridization.

In summary, this work reports a preliminary method capable of detecting and exploring genetic markers composed of midsequence SNPs and multiple base mismatches in unmodified DNA sequences. The SERS approach provides both a robust detection rubric for further analyses using polymorphisms and a useful research tool potentially capable of exploring precise biochemical changes associated with DNA mutations. Future approaches will be developed to enhance the speed and efficiency of this process. Experiments will be attempted to define minimum hybridization times and to create automated microarrays or microfluidic formats that further improve efficiency by using continuous or large batch processing designs.

Acknowledgments

G.S.M. and B.M. would like to thank North Carolina State University College of Engineering for funding. The authors declare no competing interests.

References

1. M. Claustres, "Frequency and nature of mutations and the methods to detect them," in *Guide to Mutation Detection*, G. R. Taylor and I. N. Day, Eds., pp. 9–10, John Wiley & Sons, Hoboken, NJ (2005).
2. S. Dudoit and M. J. van der Laan, "Genetic mapping of complex human traits using single nucleotide polymorphisms: the ObeLinks project," in *Multiple Testing Procedures with Applications to Genomics*, p. 489 Springer, New York (2008).
3. J. L. Parsons, E. Boswell, and G. L. Dianov, "Processing of 3'-end modified DNA strand breaks induced by oxidative damage," in *Oxidative Damage to Nucleic Acids*, M. D. Evans and M. S. Cooke, Eds., pp. 81–90, Springer, New York (2007).

4. A. Syvanen and H. Soderlund, "DNA sandwiches with silver and gold," *Nat. Biotechnol.* **20**, 349–350 (2002).
5. K. Sato, M. Sawayanagi, K. Hosokawa, and M. Maeda, "Single-base mutation detection using neutravidin-modified polystyrene nanoparticle aggregation," *Anal. Sci.* **20**, 893–894 (2004).
6. Y. C. Cao, R. Jin, and C. A. Mirkin, "Nanoparticles with Raman spectroscopic fingerprints for DNA and RNA detection," *Science* **297**, 1536–1540 (2002).
7. B. Prescott, W. Steinmetz, and G. J. J. Thomas, "Characterization of DNA structures by laser Raman spectroscopy," *Biopolymers* **23**, 235–256 (1984).
8. K. Kneipp, H. Kneipp, V. B. Kartha, R. Manoharan, G. Deinum, I. Itzkan, R. R. Dasari, and M. S. Feld, "Detection and identification of a single DNA base molecule using surface-enhanced Raman scattering (SERS)," *Phys. Rev. E* **57**, R6281–R6284 (1998).
9. S. C. Erfurth and W. L. Peticolas, "Melting and premelting phenomenon in DNA by laser Raman scattering," *Biopolymers* **14**, 247–264 (1975).
10. H. Deng, V. A. Bloomfield, J. M. Benevides, and G. J. J. Thomas, "Structural basis of polyamine-DNA recognition: spermidine and spermine interactions with genomic B-DNAs of different GC content probed by Raman spectroscopy," *Nucleic Acids Res.* **28**, 3379–3385 (2000).
11. G. D. Pitt, D. N. Batchelder, R. Bennett, R. W. Borrett, I. P. Hayward, B. J. E. Smith, K. P. J. Williams, Y. Y. Yang, K. J. Baldwin, and S. Webster, "Engineering aspects and applications of the new Raman instrument," *IEE Proc.: Sci., Meas. Technol.* **152**, 241–318 (2005).
12. L. Lafleur, J. Rice, and G. J. J. Thomas, "Raman studies of nucleic acids. VII. poly A. poly U and poly G. poly C," *Biopolymers* **11**, 2423–2437 (1972).
13. L. Sun, C. Yu, and J. Irudayaraj, "Raman multiplexers for alternative gene splicing," *Anal. Chem.* **80**, 3342–3349 (2008).
14. T. Vo-Dinh, D. L. Stokes, G. D. Griffin, M. Volkan, U. J. Kim, and M. I. Simon, "Surface-enhanced Raman scattering (SERS) method and instrumentation for genomics and biomedical analysis," *J. Raman Spectrosc.* **30**, 785–793 (1999).
15. S. E. J. Bell and N. M. S. Sirimuthu, "Surface-enhanced Raman spectroscopy (SERS) for submicromolar detection of DNA/RNA mononucleotides," *J. Am. Chem. Soc.* **128**, 15580–15581 (2006).
16. T. Vo-Dinh, L. R. Allain, and D. L. Stokes, "Cancer gene detection using surface-enhanced Raman scattering (SERS)," *J. Raman Spectrosc.* **33**, 511–516 (2002).
17. L. R. Allain and T. Vo-Dinh, "Surface-enhanced Raman scattering detection of the breast cancer susceptibility gene BRCA1 using a silver-coated microarray platform," *Anal. Chim. Acta* **469**, 149–154 (2002).
18. B. Moody and G. S. McCarty, "Statistically significant Raman detection of midsequence single nucleotide polymorphisms," *Anal. Chem.* **81**, 2013–2016 (2009).
19. S. Park, A. A. Lazarides, J. J. Storhoff, L. Pesce, and C. A. Mirkin, "The structural characterization of oligonucleotide-modified gold nanoparticle networks formed by DNA hybridization," *J. Phys. Chem. B* **108**, 12375 (2004).
20. S. Park, K. A. Brown, and K. Hamad-Schifferli, "Changes in oligonucleotide conformation on nanoparticle surfaces by modification with mercaptohexanol," *Nano Lett.* **4**, 1925–1929 (2004).
21. A. Barhoumi, D. Zhang, F. Tam, and N. J. Halas, "Surface-enhanced Raman spectroscopy of DNA," *J. Am. Chem. Soc.* **130**, 5523–5529 (2008).
22. C. Otto, T. J. J. van den Tweel, F. F. M. de Mul, and J. Greve, "Surface-enhanced Raman spectroscopy of DNA bases," *J. Raman Spectrosc.* **17**, 289–298 (1986).
23. N. H. Jang, "The coordination chemistry of DNA nucleosides on gold nanoparticles as a probe by SERS," *Bull. Korean Chem. Soc.* **23**, 1790–1800 (2002).
24. A. T. Tu, "Nucleic acids," in *Raman Spectroscopy in Biology: Principles and Applications*, pp. 134–173, John Wiley & Sons, New York (1982).
25. D. H. Turner, N. Sugimoto, R. Kierzek, and S. D. Dreiker, "RNA structure prediction," *Annu. Rev. Biophys. Biophys. Chem.* **17**, 167–192 (1988).
26. V. A. Bloomfield, D. M. Crothers, and I. Tinoco Jr., *Nucleic Acids: Structures, Properties, and Functions*, pp. 207–208, University Science Books, Sausalito, CA (2000).